SPERMATOGENESIS OF THE SPIDER CRAB Maja brachydactyla (Decapoda: Brachyura).

Authors' names

Carles G. Simeó[1*], Kathryn Kurtz[2], Manel Chiva[2], Enric Ribes[3] and Guiomar Rotllant[1]

Institutions

1 IRTA Sant Carles de la Ràpita

2 Departament de Ciències Fisiològiques II, Universitat de Barcelona

3 Departament de Biologia Cel·lular, Universitat de Barcelona

Short title:

Spermatogenesis of Maja brachydactyla

* Corresponding author:

Carles G. Simeó, IRTA Sant Carles de la Ràpita, Ctra. del PobleNou km 5.5, 43540, Sant Carles de la Ràpita, Spain. E-mail: carlos.garcia@irta.cat. Phone number: 0034 977 547 427, fax number: 0034 977 544 138

ABSTRACT

The present study describes spermatogenesis in a majid crab (Maja brachydactyla) using electron microscopy and reports the origin of the different organelles present in the spermatozoa. Spermatogenesis in M. brachydactyla follows the general pattern observed in other brachyuran species but with several peculiarities. Annulate lamellae have been reported in brachyuran spermatogenesis during the diplotene stage of first spermatocytes, the early and mid-spermatids. Unlike previous observations, a Golgi complex has been found in mid-spermatids and is involved in the development of the acrosome. The Golgi complex produces two types of vesicles: light vesicles and electron-dense vesicles. The light vesicles merge into the cytoplasm, giving rise to the proacrosomal vesicle. The electron-dense vesicles are implicated in the formation of an electron-dense granule, which later merges with the proacrosomal vesicle. In the late spermatid, the endoplasmic reticulum and the Golgi complex degenerate and form the structures-organelles complex found in the spermatozoa. At the end of spermatogenesis, the materials in the proacrosomal vesicle aggregate in a two-step process, forming the characteristic concentric three-layered structure of the spermatozoon acrosome. The newly formed spermatozoa from testis show the typical brachyuran morphology.

Key words:

Sperm morphology, gametogenesis, germ cells, ultrastructure, Majidae

INTRODUCTION

The brachyuran spermatozoon is characterized by a globular shape, the absence of a flagellum, and the presence of a variable number of radial arms (Felgenhauer and Abele, 1991). Numerous morphological and taxonomic studies have provided a clear description of the ultrastructure of the sperm cell (Jamieson and Tudge, 2000). The brachyuran spermatozoon is composed of a cup-shaped nucleus with lateral arms and decondensed chromatin, a thin cytoplasmic layer, and a complex globular acrosome, which is centrally penetrated by the perforatorium. In addition, the role of several spermatozoon components has been proposed, while others, such as the different acrosome layers, still remain unclear. Thus, the decondensed chromatin seems to provide the necessary malleability for the acrosome reaction (Krol et al., 1992; Kurtz et al., 2008), the lateral arms may participate in the attachment to the egg, and the perforatorium may play a key role during egg penetration (Brown, 1966; Hinsch, 1971; Goudeau, 1982; Medina, 1992; Medina and Rodríguez, 1992a).

Despite all the information available on the spermatozoal morphology and ultrastructure, little is known about spermatogenesis in brachyurans. The first descriptions of spermatogenesis were done using light microscopy in Menippe mercenaria (Binford, 1913), Cancer magister (Fasten, 1918), Cancer sp. (Fasten, 1924), Lophopanopeus bellus (Fasten, 1926), Sartoriana spinigera (Nath, 1932, as Paratelphusa), Eriocheir sinensis (Hoestlandt, 1948), and Scylla sp. (Estampador, 1949). However, these works revealed only the general pattern of spermatogenesis. Later, studies using transmission electron microscopy (TEM) were not conclusive and mainly described the last phases of spermatogenesis (spermiogenesis) in a few brachyuran species: Eriocheir japonicus (Yasuzumi, 1960),

Carcinus maenas (Pochon-Masson, 1962; 1968), Cancer sp. (Langreth, 1969), Pinnixa sp. (Reger, 1970), Eriocheir sinensis (Du et al., 1988), Uca tangeri (Medina and Rodríguez, 1992b), Portunus trituberculatus (Li, 1995), Scylla serrata (Wang et al., 1997b), and Sinopotamon yangtsekiense (Wang et al., 1999). While in some animal species a transverse section of the testis contains most stages of spermatogenesis (Beninger and Pennec, 1991; Patiño and Redding, 2000; Sasso-Cerri et al., 2004; Cledón et al., 2005; Thongkukiatkul et al., 2008), in brachyurans, cells belonging to the same transverse section of the testis are usually in the same stage of development (Krol et al., 1992). Therefore, obtaining the complete sequence of stages throughout spermatogenesis is a difficult task that would explain why so little information is available in brachyurans. Recent studies have revealed new features of the brachyuran spermiogenesis, such as the maturation of the spermatids in the vas deferens and seminal receptacles of the snow crab Chionoecetes opilio (Sainte-Marie and Sainte-Marie, 1999a, b) and the loss of a glycocalyx in the spermatozoa of Inachus phalangium in the seminal receptacle of the females (Rorandelli et al., 2008).

The spider crab Maja brachydactyla is an important commercial species in the Atlantic Ocean (Freire et al., 2002) that has been often synonymized with Maja squinado. Recently, its taxonomic status has been clarified (Neumann, 1998; Sotelo et al., 2008), recognizing the Mediterranean M. squinado and the Atlantic M. brachydactyla as different species. Only a few studies focused on the morphology of the reproductive system (Mouchet, 1931; Neumann, 1996 as M. squinado; Simeó et al., 2009a), spermatogenesis (Meusy, 1972 as M. squinado), and the spermatozoal ultrastructure (Tudge and Justine, 1994 as M. squinado; Simeó et al., 2009b). In the present study, we give a detailed description of spermatogenesis in the spider crab, M. brachydactyla, using TEM.

MATERIAL AND METHODS

Twenty-four adult males of Maja brachydactyla Balss, 1922 were captured in Galicia, NW Spain, by artisanal coastal fishery using gillnets between November 2006 and July 2007. The specimens were transported in dry and high humidity conditions to IRTA (Institut de Recerca i Tecnologia Agroalimentàries) facilities (Tarragona, NE Spain). Prior to dissection, carapace length (CL) and weight (W) were measured, being in average CL= 155.55 ± 6.89 mm and W= 1,147.5 ± 218.4 g (mean ± SD). Then, spider crabs were anesthetized on ice for at least 10 min until the individuals did not respond to external stimuli; heart was dissected causing the death of the animal, and pieces of testis were extracted and processed for light microscopy (LM) and TEM. The experimental procedure conforms to the current animal protection regulations (86/609/CEE, RD 1201/2005, and D 214/1997).

For LM, the right testis of three animals was extracted and divided into three parts (distal, median, and proximal to the vas deferens). The parts were fixed in Bouin's solution for 24-48 hours and then rinsed and stored in 70% ethanol until processing. Samples were dehydrated through a graded series of alcohol and embedded in paraffin. Slides of 3 µm were cut on a Leica RM 2155 rotary microtome and stained with Harris's hematoxylin-eosin (H-E) dye. Sections were photographed using an Olympus DP70 camera connected to an Olympus BX61 light microscope.

For TEM, small pieces of testis belonging to the twenty-four males were extracted and fixed in a mixture of 2% paraformaldehyde and 2.5% glutaraldehyde in cacodylate buffer (0.1 mol L^{-1}, pH 7.4) for 24 h at 4ºC. Samples were rinsed in cacodylate buffer several times, postfixed in 1% osmium tetroxide at 4ºC, dehydrated in graded series of acetone, and

105 embedded in Spurr's resin. Semithin sections, used for LM, were stained using toluidine
106 blue and observed with an Olympus BX61 light microscope. Ultrathin sections were made
107 in a Leica UCT ultramicrotome and counterstained with uranyl acetate and lead citrate.
108 Observations were made with a Jeol EM-1010 transmission electron microscope at 80 kV.
109 Sagittal sections of the germ cells were selected and measured using an image analyzing
110 system (AnalySIS, SIS; n= 15, except for early spermatid, in which only 4 sections were
111 properly oriented). The measurements of mid- and late spermatids were made using the
112 longest axis of the cell, because these stages present an oval shape. For late spermatids,
113 which show irregular nuclear shapes, nuclear measurement refers to thickness of the
114 nucleus in the sagittal section.

115 RESULTS

116 Spermatogenesis in the seminiferous tubule

117 Testes of Maja brachydactyla consist of a single seminiferous tubule, which is divided in
118 transverse section by epithelial cells into 3 zones: germinal, transformation, and evacuation
119 zones (Fig. 1). Each zone contains different stages of germ cells accompanied by accessory
120 cells and plays a different role in spermatogenesis. The germinal zone (GZ) is located at
121 one side in a transverse section of the seminiferous tubule and contains spermatogonia. The
122 transformation zone (TZ) fills the central region of the seminiferous tubule and contains the
123 different stages of spermatogenesis, from spermatocytes to spermatozoa. As cells belonging
124 to the same transverse section are usually in the same stage of development or in two
125 successive stages, independently of their distance to the vas deferens, we had to dissect a
126 large number of animals to follow the spermatogenesis along the seminiferous tubule. The
127 evacuation zone (EZ) is diametrically opposed to the GZ and only contains mature

spermatozoa originating from the TZ. The EZ collects and transports spermatozoa produced along the testis towards the vas deferens, where they are packed and stored in spermatophores. Hence, we have focused our observations on the TZ because it is the place where spermatogenesis takes place.

Spermatocyte stages

Primary spermatocytes are spherical cells with a spherical nucleus located in the central region of the cell (Figs. 2 and 3A-D). Spermatocytes are the largest germ cells measured in this study (Table 1) and their size and nuclei remains constant during meiotic divisions.

Preleptotene spermatocytes show nuclei with small clumps of heterochromatin (Fig. 2A). The cytoplasm appears homogeneous, with granular material and few organelles. The mitochondria are distributed throughout the cytoplasm, containing slightly electron-dense material and few, poorly developed cristae. The endoplasmic reticulum (ER) is composed of isolated, irregular cisternae containing material of low electron-density.

Leptotene spermatocytes contain individualized chromosomes condensed into strands (see arrowheads in Fig. 2B,C) and a single nucleolus in the nucleus (Fig. 2B). The cytoplasm exhibits a concentric membrane system, which is composed of flattened concentric cisternae, and an oval-shaped, slightly prominent, electron-dense nucleolus-like body or nuage (Fig. 2C).

In the pachytene stage, spermatocytes show paired chromosomes with synaptonemal complexes (arrowheads and inset in Fig. 2 D). In the cytoplasm, the concentric membrane system shows lateral dilatations associated to the peripheral cisternae (asterisks in Fig. 2E). The nuage is still present (Fig. 2D), although it is larger and less electron-dense than in the leptotene stage.

In the diplotene stage, chromosomes are paired and condensed (Fig. 3A), and the synaptonemal complexes are still present (Fig. 3D). Elongated membrane cisternae merge in the cytoplasm, forming concentric complexes that contain mitochondria (Fig. 3C). In addition, the cytoplasm contains annulate lamellae, which are composed of several parallel membrane layers that eventually become associated to the nucleus (Fig. 3B,D). The nuage increases in size, appearing as a prominent electron-dense body in the cytoplasm (Fig. 3B).

Secondary spermatocytes in prophase II have condensed chromosomes (Fig. 3E) and a light electron-dense nucleoplasm. The cytoplasm is less electron-dense than in the previous stage and contains the nuage and several irregular ER cisternae with light electron-dense material.

For the following secondary spermatocyte stages, we did not obtain sections for TEM; therefore in the next section the description of spermatogenesis continues with spermatid maturation.

The accessory cells appear closely related to spermatocytes, showing a spindle-shaped nucleus located at the center of the cell (Fig. 2B). Heterochromatin is condensed mainly in the periphery of the nucleus, and the nucleoplasm is moderately electron-dense. A nucleolus, centrally placed, is also present. The cytoplasm contains granular material and is more electron-dense when it is found between spermatocytes (arrowhead in Fig. 3A).

Spermiogenesis

Spermiogenesis shows 3 stages, early, mid- and late spermatids, according to changes in chromatin condensation, and the development and differentiation of the proacrosomal vesicle. Due mainly to morphological changes of the nucleus during the last stage (Table 1), spermatids decrease in size during spermiogenesis.

Early spermatids are slightly polarized, spherical cells with the nucleus located at one pole of the cell (here referred as nuclear pole) and the cytoplasm at the opposite pole (acrosomal pole, Fig. 4A), where the proacrosomal vesicle will arise. The nucleus is spherical and contains granular chromatin, which still appears as condensed clumps distributed throughout the nucleoplasm and is also associated to the nuclear envelope (Fig. 4A). The nuclear envelope shows nuclear pores, particularly in the region facing the acrosomal pole (arrowhead and inset in Fig. 4B). In the cytoplasm, several small mitochondria with degenerate cristae show electron-dense contents (Fig. 4B). Few concentric membranous arrangements like those observed in the diplotene stage are still present (Fig. 4A). In addition, flattened cisternae extend longitudinally resembling a poorly developed ER (Fig. 4B).

Mid-spermatids are spherical to oval cells characterized by chromatin decondensation, growth and differentiation of the ER and Golgi complex, and development of the proacrosomal vesicle. The first change observed in mid-spermatids is the decondensation of chromatin (Fig. 4C). Thus, the nucleus contains homogeneous chromatin with few small, condensed clumps (arrowhead in Fig. 4D,E). In the cytoplasm, membrane layers are arranged longitudinally, while the annulate lamellae appear associated to the nuclear envelope (Fig. 4D). Later, the membrane layers continue their development and differentiate into the ER and a membranous system resembling a Golgi complex (Fig. 4E,F). The ER is composed of highly packed longitudinal cisternae oriented parallel to the nuclear envelope, while the Golgi complex, consists of a few semicircular cisternae, which produces 2 types of vesicles containing either light or electron-dense materials. Light

196 electron-dense vesicles merge in the acrosomal pole to give rise to the proacrosomal
197 vesicle, which is filled with homogeneous granular material (Fig. 4F).
198 As spermiogenesis progresses, the proacrosomal vesicle grows in parallel to the ER and
199 Golgi complex, occupying a large region of the mid-spermatid (Fig. 5A). The ER and Golgi
200 complex fill the cytoplasm, which is reduced to a band between the nucleus and the
201 proacrosomal vesicle. In addition, small mitochondria containing electron-dense material
202 are intercalated within the cisternae of the ER and Golgi complex (Fig. 5B,C). The first
203 sign of differentiation in the proacrosomal vesicle is the presence of a single electron-dense
204 granule. This electron-dense granule is a spherical vesicle delimitated by a membrane
205 (white arrows in Fig. 5C) and contains electron-dense material, which seems to originate in
206 the cytoplasm by the fusion of the electron-dense Golgi vesicles. Later, the membranes of
207 the granule and the proacrosomal vesicle merge, and the granule appears in the apical
208 region of the spermatid (Fig. 5D). Once the proacrosomal vesicle achieves its maximum
209 size, the nuclear envelope breaks in the equatorial region of the cell, and the ER and Golgi
210 complex degenerate (Fig. 5F).
211 During the mid-spermatid stage, the accessory cells show features similar to those in the
212 spermatocyte stage. In addition, the cytoplasm has a vacuolized appearance with regions of
213 different electron-densities (arrows in Fig. 4C). Some mitochondria in the accessory cells
214 appear associated to the regions of the spermatids where the ER and Golgi complex appear
215 (mitochondria pointed out with arrowhead in Fig. 5B).
216 Late spermatids demonstrate several important changes in the nuclear morphology and the
217 internal organization of the proacrosomal vesicle. Late spermatids are highly polarized
218 cells, showing a reduced, half-moon shaped nucleus at the nuclear pole and a voluminous

proacrosomal vesicle (Fig. 6A,B). The nuclear envelope merges with the plasma membrane, giving rise to a thick, electron-dense membrane (Fig. 6B,C). The cytoplasm is now highly reduced to the margins of the nucleus in the equatorial region and is filled with degenerate mitochondria and a membrane system derived from the degenerated ER and Golgi complex (Fig. 6C). A highly electron-dense band that will give rise to the operculum appears over the apical granule of the proacrosomal vesicle (Fig. 6B). In the base of the proacrosomal vesicle, a thin layer of granular material (arrowhead in Fig. 6B) covers an invagination of cytoplasm, which is the origin of the perforatorium (Fig. 6D). Later, the invagination extends anteriorly while it is surrounded by the posterior extension of the electron-dense apical granule (Fig. 6E). The maturation of the spermatids continues with the lateral extension of the nucleus, appearing as a horseshoe-shape in longitudinal section that surrounds the proacrosomal vesicle. In the apical region, the operculum extends laterally covering the perforatorium and, partially, the proacrosomal vesicle (Fig. 6E). The contents of the proacrosomal vesicle aggregate, firstly into clumps distributed throughout the vesicle and then forming a layer around the perforatorium (Fig. 6F). A homogeneous layer of light electron-dense granular material still remains in the outer region of the proacrosomal vesicle (Fig. 6G). The last modifications of the late spermatid are the development of the nuclear lateral arms in the subapical region of the cell (arrowhead in Fig. 6G) and the condensation of the outer layer of the proacrosomal vesicle.

At the end of the spermiogenesis, the accessory cells present a degenerated aspect. In the nucleus, heretochromatin and nucleoplasm are highly electron-dense (Fig. 6A). The cytoplasm, which surrounds late spermatids, also increases in electron-density, showing

241 numerous degenerate mitochondria (asterisk in Fig. 6C) and highly electron-dense spherical
242 bodies, which are probably endosomal vesicles with degradative activity (Fig. 6E).
243 The newly formed spermatozoa are transferred from the transformation to the evacuation
244 zone of the seminiferous tubule (Fig. 7A) and then moved towards the vas deferens, where
245 they are packed in spermatophores. The spermatozoon is the smallest of the germ cell
246 lineage (Table 1). It is composed of a globular acrosome, a thin layer of cytoplasm and a
247 cup-shaped nucleus with several lateral arms (Fig. 7B). The acrosome presents 3 layers of
248 different electron-density and is encircled in the subapical region by the structures-
249 organelles complex (SO-complex), which consists of membrane layers, degenerate
250 mitochondria and microtubules.
251 DISCUSSION
252 We present a complete sequence of stages throughout spermatogenesis of the spider crab,
253 Maja brachydactyla. Because the germ cells within a cross section of the seminiferous
254 tubule in were all in the same stage or two successive stages, the differentiation of the germ
255 cells had to be followed along the testis. Our work complements previous ultrastructural
256 studies in brachyurans that were focused on spermiogenesis (Yasuzumi, 1960; Pochon-
257 Masson, 1968; Langreth, 1969; Reger, 1970; Du et al., 1988; Medina and Rodríguez,
258 1992b; Li, 1995; Wang et al., 1997b; Wang et al., 1999). All previous studies were
259 performed with the higher groups within Eubrachyura, but majids appear in the basal
260 positions within this group, and therefore the results presented here carry potential
261 phylogenetic significance (see Jamieson and Tudge, 2000 for phylogenetic discussion).
262 Contrary to former studies (Pochon-Masson, 1983) our morphological observations suggest
263 that the acrosome in M. brachydactyla is mainly derived from the Golgi-like complex.

Spermatocytes

During the early phases of spermatogenesis in M. brachydactyla, the nucleus of primary spermatocytes contains typical meiotic figures such as the synaptonemal complexes in the pachytene stage. In addition, the cytoplasm contains few mitochondria, a developing ER and other membrane arrangements, and a nuage (Du et al., 1988; Li, 1995; Wang et al., 1997b). Similar findings were also described in the cytoplasm of other decapod crustaceans, such as Pagurus bernhardus and Nephrops norvegicus (Chevaillier, 1970). In both species, as in M. brachydactyla, a low number of mitochondria with poorly developed cristae were present throughout the cytoplasm, the ER was continuous with the nuclear envelope, and the Golgi complex was absent. On the contrary, the cytoplasm of Procambarus paeninsulanus (Hinsch, 1993) shows aggregated mitochondria and an endoplasmic reticulum that breaks up into small tubular aggregates. The cytoplasm of the spermatocytes in M. brachydactyla demonstrates 3 peculiarities: the nuage, the concentric membrane system, and the annulate lamellae. The nuage appears as an electron-dense body during most primary spermatocyte stages, being especially prominent in the diplotene stage. The concentric membrane system appears in the leptotene and pachytene stages and shows lateral dilatations in pachytene. The annulate lamellae appear during diplotene, and to our knowledge this is the first report of annulate lamellae in the spermatocytes of a crab. Annulate lamellae are described as a network of parallel intracytoplasmic membranes observed in dividing cells, both somatic and germ cells (Kessel, 1992). Their origin and function is still unclear, although recent immunolocalization studies have indicated that the annulate lamellae may act as a reservoir of nuclear envelope and nuclear pore complex proteins (Imreh and Hallberg, 2000).

Spermiogenesis

The basic changes occurring during spermiogenesis were established using light microscopy. These events were summarized as follows: 1) cellular polarization due to the marginalization of the nucleus, along with the development of the proacrosomal vesicle; 2) formation of a ring by the membranous system; 3) development of the operculum and perforatorium in the acrosomal vesicle; 4) nuclear surrounding of the acrosome; and 5) development of the radial arms (Binford, 1913; Fasten, 1918; 1926; Nath, 1932). Later studies using transmission electron microscopy (Yasuzumi, 1960; Pochon-Masson, 1962; 1968; Langreth, 1969; Reger, 1970; Du et al., 1988; Medina and Rodríguez, 1992b; Li, 1995; Wang et al., 1997b; Wang et al., 1999), including the present work, support these findings.

The first change occurring during spermiogenesis in M. brachydactyla is the decondensation of chromatin in the mid-spermatid. The decondensation leads to a nucleus with slightly condensed, fibrillar chromatin, which is highly characteristic of the brachyuran spermatozoon. Similar results have been described at the beginning of spermiogenesis in Cancer sp. (Langreth, 1969) and Pinnixia sp. (Reger, 1970), where chromatin condensed in clumps appeared in the periphery of the nucleus. However, the nucleus of Uca tangeri (Medina and Rodríguez, 1992b) presented a granular homogeneous appearance. The molecular basis of chromatin decondensation has largely been investigated. The first studies concluded that the chromatin in decapod spermatozoa was not associated to proteins, because neither histones nor protamines were detected (Vaughn and Locy, 1969; Vaughn and Hinsch, 1972; Vaughn and Thomson, 1972). Recently, a low histone to DNA ratio and a high level of acetylation of these proteins were reported in

Cancer sp. (Kurtz et al., 2008) and M. brachydactyla (Kurtz et al., 2009), which could explain the decondensed chromatin in these species.

Other changes in the nucleus include breakage of the nuclear envelope and a dramatic modification of its morphology. During spermiogenesis in M. brachydactyla, the nuclear envelope disintegrates near the basal region of the acrosome, similarly to Carcinus maenas (Pochon-Masson, 1968), Cancer sp. (Langreth, 1969), Pinnixa sp. (Reger, 1970), and U. tangeri (Medina and Rodríguez, 1992b). As a result, the chromatin is in contact with the cytoplasm, giving rise to the so-called nucleo-cytoplasm complex. In addition, the nuclear envelope in M. brachydactyla also gives rise to a pentalaminar system when it fuses with the plasma membrane, as has been observed in several brachyurans (Brown, 1966; Langreth, 1969; Reger, 1970; Medina and Rodríguez, 1992b). The nucleus is also subjected to deep morphological changes during spermiogenesis, going from spherical in early and mid-spermatids to half-moon and, finally, horseshoe-shaped in late spermatids. During this process, the nucleus extends anteriorly, surrounding the acrosome and developing the nuclear lateral arms, as described for C. maenas and U. tangeri (Pochon-Masson, 1968; Medina and Rodríguez, 1992b). Nothing is known about the mechanism of the morphological modification of the nucleus and the development of the lateral arms. The lateral arms are usually associated to the membrane and mitochondrial complex of the spermatozoa, and they are sustained by microtubules in some species, such as C. maenas (Pochon-Masson, 1965), Libinia emarginata (Hinsch, 1969), and Mithrax sp. (Hinsch, 1973).

Throughout spermiogenesis in M. brachydactyla, the cytoplasm becomes highly reduced until it is finally limited to a thin band between the nucleus and the acrosome. The

cytoplasmic reduction is due to the development of the acrosome and, probably, to the release of cytoplasmic regions, which is especially intense at the end of spermiogenesis. In E. japonicus (Yasuzumi, 1960), large regions of the cytoplasm become isolated and slough off. As reported for C. maenas (Pochon-Masson, 1968) and Cancer sp. (Langreth, 1969), the accessory or nurse cells play a key role in phagocytosing and degrading the spermatid residual cytoplasm. The accessory cells could also play a similar role in M. brachydactyla, as suggested by the presence of electron-dense spherical bodies (probably endosomal vesicles with degradative activity) in their cytoplasm at the end of spermiogenesis.

The different organelles are also modified during spermiogenesis. As described for U. tangeri (Medina and Rodríguez, 1992b), the mitochondria in M. brachydactyla are scarce and with degenerate cristae. During spermiogenesis, mitochondria undergo a process of aggregation and number reduction by means of fusion or cristae degeneration (Wang et al., 1997a), which in some cases leads to a loss of their oxidative function (Pearson and Walker, 1975). At the end of the spermiogenesis in M. brachydactyla, the mitochondria are integrated in the structures-organelles (SO) complex of the spermatozoa, as shown for several species (Pochon-Masson, 1962; Langreth, 1969; Reger, 1970; Medina and Rodríguez, 1992b).

The ER, Golgi complex, and other cytoplasmic membrane are also subjected to extensive morphological modifications during the spermiogenesis in M. brachydactyla. During spermiogenesis, the cytoplasmic membrane systems progressively develop and differentiate into the ER and the Golgi complex. The presence of annulate lamellae during the mid-spermatid stage suggests that the ER could develop from the annulate lamellae themselves, as documented during the spermiogenesis in Drosophila sp. (Merisko, 1989). Once the

proacrosomal vesicle reaches its maximum size, the ER and the Golgi complex degenerate into a membrane system that occupies the equatorial region of the cell at the end of the mid-spermatid stage. Later, the membrane system together with the mitochondria is pushed towards the apical portion of the late spermatid and gives rise in the spermatozoa to the SO-complex. The origin of the SO-complex (synonymous with membranous organelle (Reger, 1970), nucleo-chondrio-polymicrotubular complex (complex nucléochondriomique, Pochon-Masson, 1968), membrane complex (Langreth, 1969; Du et al., 1988; Li, 1995; Wang et al., 1999), membranous lamellar complex (Chiba et al., 1992), and membranous lamellae (Medina and Rodríguez, 1992b)) has been previously attributed to ER cisternae (Langreth, 1969; Du et al., 1988; Li, 1995) or a nuclear and ER origin (Reger, 1970). Aside its origin, the SO-complex is composed of a membrane system, mitochondria, and occasionally microtubules (Krol et al., 1992).

Our observations suggest that the acrosome in M. brachydactyla is suggested to be derived from the vesicles of a putative Golgi complex, similarly to that observed in Sinopotamon yangtsekiense (Wang et al., 1999). At the mid-spermatid stage, a cytoplasmic membrane system morphologically similar to a Golgi complex produces two kinds of vesicles that give rise to the acrosome. These results contrast to most of previous morphological studies, in which the origin of the acrosome was ascribed to the ER or nuclear envelope derivatives (Pochon-Masson, 1983). More recently, Tudge (2009) has proposed that the Golgi complex described in S. yangtsekiense and Macrobrachium nipponense could represent Golgi-like extensions of the ER. However, the Golgi complex has been indirectly demonstrated during the spermiogenesis of Eriocheir sinensis by means of the detection two proteins, kinesin KIFC1 and GM130 protein, specifically associated to the Golgi complex (Yu et al., 2009).

379 Since no typical Golgi complex has been described in morphological studies (Du et al.,
380 1988), Yu et al. (2009) proposed that the Golgi complex in E. sinensis may be composed of
381 single Golgi stacks (Yu et al., 2009). Thus, it seems that if the Golgi complex is present in
382 the spermatids of brachyurans, it may show a complex morphology, difficult to identify.
383 Here, we present a membrane system as candidate to Golgi complex, although
384 immunocytochemical studies linking morphology and function might be needed to confirm
385 its nature.
386 The Golgi complex produces two kinds of vesicles that contain either light or electron-
387 dense material. Thus, the acrosome is formed from the combination of the proacrosomal
388 vesicle and an electron-dense granule, which are respectively originated by the fusion of the
389 light and electron-dense Golgi vesicles. The electron-dense granule has been also reported
390 in other species (Pochon-Masson, 1968; Langreth, 1969; Medina and Rodríguez, 1992b),
391 but its origin has not been determined. Later, the electron-dense granule migrates towards
392 the apical region of the proacrosomal vesicle and, finally, extends posteriorly surrounding
393 the perforatorium or adjacent areas, as occurs for several species (Pochon-Masson, 1983;
394 Krol et al., 1992). As described for U. tangeri (Medina and Rodríguez, 1992b), the
395 operculum develops above the granule as a thin, highly electron-dense band. Following the
396 extension of the electron-dense granule, the development of the perforatorium begins in the
397 basal region of the acrosome. A layer of granular material, known as the granular belt
398 (Langreth, 1969; Medina and Rodríguez, 1992b), appears at the base of the proacrosomal
399 vesicle. Simultaneously, an invagination, which will develop into the perforatorium,
400 follows the central axis of the proacrosomal vesicle, from the posterior end towards the
401 apical region. As in Cancer sp., the electron-dense granule in M. brachydactyla grows

posteriorly surrounding the perforatorium up to its base (Langreth, 1969). The last event in the proacrosomal vesicle is the aggregation of the acrosomal materials. In M. brachydactyla, this process occurs in two stages. First, the materials condense throughout the proacrosomal vesicle, and second, the materials surround the central axis. However, an outer layer of uncondensed material remains until the expansion of the nucleus, which is the last step of spermatid differentiation. As a result of this two-step aggregation, the acrosome of M. brachydactyla contains three layers disposed in a concentric pattern. Previous studies did not describe the aggregation pattern in the acrosome, since those species did not exhibit a three-layered acrosome (Yasuzumi, 1960; Pochon-Masson, 1968; Langreth, 1969; Reger, 1970; Du et al., 1988; Medina and Rodríguez, 1992b; Li, 1995; Wang et al., 1997b; Wang et al., 1999).

In conclusion, the ultrastructural study of spermatogenesis in M. brachydactyla has revealed the presence of annulate lamellae in the spermatocyte, early and mid-spermatids, the presence of a putative Golgi complex involved in the acrosome formation, and a two-step aggregation process of the acrosomal contents.

418 ACKNOWLEGMENTS

419 The authors thank Núria Cortadellas and Almudena Garcia for their technical support
420 (Unitat de Microscòpia Electrònica, Universitat de Barcelona). C.G.S. was supported by the
421 University and Research Commission of the Innovation, University and Company
422 Department of the Catalonian Government. G.R. thanks the Ramon y Cajal Program of the
423 Spanish Ministry of Science and Innovation. This study has been supported by the Spanish
424 Ministry of Environment and Rural and Marine Areas (JACUMAR), the Spanish Ministry
425 of Science and Innovation (BFU 2005-00123 grant), the Catalonian Government (Xarxa de
426 Referència i Desenvolupament en Aqüicultura) and the FEDER funding.

427 LITERATURE CITED

428 Beninger PG, Pennec Ml. 1991. Functional anatomy of scallops. In: Shumway SE, editor.
429 Scallops: biology, ecology and aquaculture. Amsterdam: Elsevier. p 133-233.

430 Binford R. 1913. The germ-cells and the process of fertilization in the crab, Menippe
431 mercenaria. J Morphol 24:147-201.

432 Brown GG. 1966. Ultrastructural studies of sperm morphology and sperm-egg interaction
433 in the decapod Callinectes sapidus. J Ultra Res 14:425-440.

434 Chevaillier P. 1970. Recherches sur la structure et les constituants chimiques des cellules
435 germinales mâles des crustacés décapodes [PhD thesis]. Rennes: Université de
436 Rennes. 322 p.

437 Chiba A, Kon T, Honma Y. 1992. Ultrastructure of the spermatozoa and spermatophores of
438 the zuwai crab, Chionoecetes opilio (Majidae, Brachyura). Acta Zool 73:103-108.

439 Cledón M, Arntz W, Penchaszadeh PE. 2005. Gonadal cycle in an Adelomelon brasiliana
440 (Neogastropoda: Volutidae) population of Buenos Aires province, Argentina. Mar
441 Biol 147:439-445.
442 Du N, Xue L, Lai W. 1988. Studies on the sperm of Chinese mitten-handed crab, Eriocheir
443 sinensis (Crustacea, Decapoda). 2. Spermatogenesis. Oceanol Limnol Sinica 19:71-
444 75.
445 Estampador EP. 1949. Scylla (Crustacea: Portunidae) II. Comparative studies on
446 spermatogenesis and oogenesis. Philip Jour Sci 78:95-109.
447 Fasten N. 1918. Spermatogenesis of the pacific coast edible crab, Cancer magister Dana.
448 Biol Bull 34:277-307.
449 Fasten N. 1924. Comparative stages in the spermatogenesis of various Cancer crabs. J
450 Morphol 39:47-61.
451 Fasten N. 1926. Spermatogenesis of the black-clawed crab, Lophopanopeus bellus
452 (Stimpson) Rathburn. Biol Bull 50:277-293.
453 Felgenhauer BE, Abele LG. 1991. Morphological diversity of decapoda spermatozoa. In:
454 Bauer RT, Martin JW, editors. Crustacean Sexual Biology. New York: Columbia
455 University Press. p 322-339.
456 Freire J, Bernárdez C, Corgos A, Fernández L, González- Gurriarán E, Sampedro MP,
457 Verísimo P. 2002. Management strategies for sustainable invertebrate fisheries in
458 coastal ecosystems of Galicia (NW Spain). Aquatic Ecol 36:41-50.
459 Goudeau M. 1982. Fertilization in a crab .1. Early events in the ovary, and cytological
460 aspects of the acrosome reaction and gamete contacts. Tissue Cell 14:97-111.

461 Hinsch GW. 1969. Microtubules in the sperm of the spider crab, Libinia emarginata L. J
462 Ultra Res 29:525-534.
463 Hinsch GW. 1971. Penetration of the oocyte envelope by spermatozoa in the spider crab. J
464 Ultra Res 35:86-97.
465 Hinsch GW. 1973. Sperm structure of Oxyrhyncha. Can J Zool 51:421-426.
466 Hinsch GW. 1993. Ultrastructure of spermatogonia, spermatocytes, and sertoli cells in the
467 testis of the crayfish, Procambarus paeninsulanus. Tissue Cell 25:737-742.
468 Hoestlandt H. 1948. Recherches sur la biologie de l'Eriocheir sinensis en France. Ann Ins
469 Oceanogr 24:1-116.
470 Imreh G, Hallberg E. 2000. An integral membrane protein from the nuclear pore complex is
471 also present in the annulate lamellae: implications for annulate aamella formation.
472 Experimental Cell Research 259:180-190.
473 Jamieson BGM, Tudge CC. 2000. Progress in male gamete ultrastructure and phylogeny.
474 In: Adiyodi KG, Adiyodi RG, editors. Reproductive Biology of Invertebrates.
475 Kerala: John Wiley and Sons. p 1-95.
476 Kessel RG. 1992. Annulate lamellae: a last frontier in cellular organelles. In: Kwang
477 WJaMF, editor. International Review of Cytology: Academic Press. p 43-120.
478 Krol RM, Hawkins WE, Overstreet RM. 1992. Reproductive components. In: Harrison FW,
479 Humes AG, editors. Microscopic Anatomy of Invertebrates. New York: Wiley-Liss,
480 Inc. p 295-343.
481 Kurtz K, Ausió J, Chiva M. 2009. Preliminary study of sperm chromatin characteristics of
482 the brachyuran crab Maja brachydactyla. Histones and nucleosome-like structures in

483 decapod crustacean sperm nuclei previously described without SNBPs. Tissue Cell
484 doi:10.1016/j.tice.2009.02.003.
485 Kurtz K, Martínez-Soler F, Ausió J, Chiva M. 2008. Histones and nucleosomes in Cancer
486 sperm (Decapod: Crustacea) previously described as lacking basic DNA-associated
487 proteins: A new model of sperm chromatin. J Cell Biochem 105:574-584.
488 Langreth SG. 1969. Spermiogenesis in cancer crabs. J Cell Biol 43:575-603.
489 Li TW. 1995. On spermatogenesis and sperm ultrastructure of blue crab Portunus
490 trituberculatus (Crustacea, Decapoda). Acta Zool Sinica 41:41-47.
491 Medina A. 1992. Structural modifications of sperm from the fiddler crab Uca tangeri
492 (Decapoda) during early stages of fertilization. J Crustacean Biol 12:610-614.
493 Medina A, Rodríguez A. 1992a. Structural changes in sperm from the fiddler crab, Uca
494 tangeri (Crustacea, Brachyura), during the acrosome reaction. Mol Reprod Dev
495 33:195-201.
496 Medina A, Rodríguez A. 1992b. Spermiogenesis and sperm structure in the crab Uca
497 tangeri (Crustacea, Brachyura), with special reference to the acrosome
498 differentiation. Zoomorphology 111:161-165.
499 Merisko EM. 1989. Annulate lamellae: an organelle in search of a function. Tissue Cell
500 21:343-354.
501 Meusy MJ-J. 1972. La gamétogenèse et la fraction protéique de l'hémolymphe spécifique
502 du sexe femelle chez quelques Crustacés supérieurs: étude descriptive et rôle des
503 glandes androgènes [PhD Thesis]. Paris: Universite Paris VI. 165 p.

504 Mouchet S. 1931. Spermatophores des Crustacés Décapodes Anomures et Brachyoures et
505 castration parasitaire chez quelques Pagures. Ann Sta Océanogr Salammbô VI:1-
506 203.
507 Nath V. 1932. Spermatid and sperm in Paratelphusa spinigera. Q J Microsc Sci 229:543-
508 556.
509 Neumann V. 1996. Comparative gonopod morphology of the European spider crabs of the
510 genus Maja Lamarck 1801. Senckenb Biol 75:143-157.
511 Neumann V. 1998. A review of the Maja squinado (Crustacea: Decapoda: Brachyura)
512 species-complex with a key to the eastern Atlantic and Mediterranean species of
513 genus. J Nat Hist 32:1667-1684.
514 Patiño R, Redding JM. 2000. Reproductive systems. In: Ostrander GK, editor. The
515 laboratory fish. London: Academic Press. p 489-500.
516 Pearson PJ, Walker MH. 1975. Alteration of cytochrome-C oxidase activity during
517 spermatogenesis in Carcinus maenas. Cell Tissue Res 164:401-410.
518 Pochon-Masson J. 1962. Le chondriofusome des gamètes males du Crustacé Décapode
519 Carcinus maenas. C R Acad Sci Paris 254:4076-4078.
520 Pochon-Masson J. 1965. L'ultrastructure des épines du spermatozoïde chez les décapodes
521 (Macroures, Anomoures, Brachyoures). C R Acad Sci Paris 260:3762-3764.
522 Pochon-Masson J. 1968. L'ultrastructure des spermatozoïdes vésicularies chez les crustacés
523 décapodes avant et au cours de leur dévegination expérimentale. I. Brachyoures et
524 Anomoures. Ann Sci Nat Zool 10:1-100.

525 Pochon-Masson J. 1983. Spermatogenesis and sperm function. In: Adiyodi KG, Adiyodi
526 RG, editors. Reproductive Biology of Invertebrates. Kerala: John Wiley and Sons
527 Ltd. p 407-449.
528 Reger JF. 1970. Studies on the fine structure of spermatids and spermatozoa of the crab,
529 Pinnixia sp. J Morphol 132:89-100.
530 Rorandelli R, Paoli F, Cannicci S, Mercati D, Giusti F. 2008. Characteristics and fate of the
531 spermatozoa of Inachus phalangium (Decapoda, Majidae): Description of novel
532 sperm structures and evidence for an additional mechanism of sperm competition in
533 Brachyura. J Morphol 269:259-271.
534 Sainte-Marie G, Sainte-Marie B. 1999a. Reproductive products in the adult snow crab
535 (Chionoecetes opilio). I. Observations on spermiogenesis and spermatophore
536 formation in the vas deferens. Can J Zool 77:440-450.
537 Sainte-Marie G, Sainte-Marie B. 1999b. Reproductive products in the adult snow crab
538 (Chionoecetes opilio). II: Multiple types of sperm cells and of spermatophores in
539 the spermathecae of mated females. Can J Zool 77:451-462.
540 Sasso-Cerri E, De Faria FP, Freymuller E, Miraglia SM. 2004. Testicular morphological
541 changes during the seasonal reproductive cycle in the bullfrog Rana catesbeiana. J
542 Exp Zoolog A Comp Exp Biol 301A:249-260.
543 Simeó CG, Ribes E, Rotllant G. 2009a. Internal anatomy and ultrastructure of the male
544 reproductive system of the spider crab Maja brachydactyla (Decapoda: Brachyura).
545 Tissue Cell doi:10.1016/j.tice.2009.02.002.
546 Simeó CG, Kurtz K, Rotllant G, Chiva M, Ribes E. 2009b. Sperm ultrastructure of the
547 spider crab Maja brachydactyla (Decapoda: Brachyura). J Morphol.

548 Sotelo G, Morán P, Posada D. 2008. Genetic identification of the northeastern Atlantic
549 spiny spider crab as Maja brachydactyla Balss, 1922. J Crustacean Biol 28:76-81.
550 Thongkukiatkul A, Jungudomjaroen S, Ratanapahira C. 2008. Spermatogenesis and
551 chromatin condensation in male germ cells of sea cucumber Holothuria leucospilota
552 (Clark, 1920). Tissue Cell 40:167-175.
553 Tudge CC. 2009. Spermatozoal morphology and its bearing on decapod phylogeny. In:
554 Martin JW, Crandall KA, Felder DL, editors. Crustacean Issues 18: Decapod
555 Crustacean Phylogenetics. Boca Raton, Florida: CRC Press, Taylor & Francis
556 Group. p 101-119.
557 Tudge CC, Justine JL. 1994. The cytoskeletal proteins actin and tubulin in the spermatozoa
558 of 4 decapod crabs (Crustacea, Decapoda). Acta Zool 75:277-285.
559 Vaughn JC, Locy RD. 1969. Changing nuclear histone patterns during development. III:
560 The deoxyribonucleic acid content of spermatogenic cells in the crab Emerita
561 analoga. J Histochem Cytochem 17:591-600.
562 Vaughn JC, Hinsch GW. 1972. Isolation and characterization of chromatin and DNA from
563 the sperm of the spider crab, Libinia emarginata. J Cell Sci 11:131-152.
564 Vaughn JC, Thomson LA. 1972. A kinetic study of DNA and basic protein metabolism
565 during spermatogenesis in the sand crab, Emerita analoga. J Cell Biol 52:322-337.
566 Wang L, Du N-S, Lai W. 1997a. Mitochondrial ultrastructure during spermatogenesis of
567 Sinopotamon yangtsekiense (Crustacea: Decapoda). Acta Zool Sinica 43:113-118.
568 Wang L, Du N-S, Lai W. 1999. Studies on spermiogenesis of a freshwater crab
569 Sinopotamon yangtsekiense (Crustacea Decapoda). Acta Hydrobiol Sinica 23:29-
570 33.

571 Wang YL, Zhang ZP, Li SJ. 1997b. Ultrastructure of spermatogenesis in the crab Scylla
572 serrata. Acta Zool Sinica 43:249-254.
573 Yasuzumi G. 1960. Spermatogenesis in animals as revealed by electron microscopy: VII.
574 Spermatid differentiation in the crab, Eriocheir japonicus. J Biophys Biochem Cytol
575 7:73-78.
576 Yu K, Hou L, Zhu J-Q, Ying X-P, Yang W-X. 2009. KIFC1 participates in acrosomal
577 biogenesis, with discussion of its importance for the perforatorium in the Chinese
578 mitten crab Eriocheir sinensis. Cell Tissue Res 337:113-123.
579

FIGURE LEGENDS

Fig. 1. Maja brachydactyla. Light microscopy of a seminiferous tubule. A. Transverse section of the seminiferous tubule divided in 3 zones: germinal, transformation, and evacuation zones. In this section, the transformation zone contains spermatids and an enlarged accessory cell. B. Epithelial layer separating the germinal and transformation zones. C. Epithelium between the transformation and evacuation zones. AC, accessory cell; Ept, epithelium; EZ, evacuation zone; GZ, germinal zone; TZ, transformation zone.

Fig. 2. Maja brachydactyla. Transmission electron micrographs of primary spermatocytes. A. Preleptotene stage. Spermatocytes showing small clumps of heterochromatin in the nucleus. The cytoplasm contains few organelles, such as mitochondria with poorly developed cristae and irregular cisternae, and vesicles of endoplasmic reticulum. B. Leptotene stage of the spermatocyte and adjacent cells. The nucleus has a single nucleolus and individualized chromosomes (arrow, also in C). A concentric membrane system appears in the cytoplasm. An accessory cell shows a spindle-shaped nucleus with a prominent nucleolus. C. Leptotene stage of the spermatocyte showing the concentric membrane system, mitochondria with poorly developed cristae, and a nuage in the cytoplasm. D. Pachytene stage of the spermatocyte showing paired chromosomes and synaptonemal complexes (arrowheads). Inset shows synaptonemal complexes at higher magnification (arrowheads). In the cytoplasm, the concentric membrane system and the nuage are more prominent. E. Pachytene stage, detail of the concentric membrane system showing lateral dilatations in the periphery (asterisks), with a small electron-dense

603 mitochondrion. AC, accessory cell; CMS, concentric membrane system; ER,
604 endoplasmic reticulum; M, mitochondria; N, nucleus; Ng, nuage; Nu, nucleolus.
605 Fig. 3. Maja brachydactyla. Transmission electron micrographs of spermatocytes. A.
606 Primary spermatocyte during diplotene of the spermatocyte showing condensed and
607 paired chromosomes in the nucleus. In the cytoplasm, the nuage is more prominent,
608 several membrane systems are organized in concentric systems, and the annulate
609 lamellae are present. The cytoplasm of the accessory cells (arrowhead) appears as a
610 highly electron-dense material. B. Detail of the cytoplasm showing the annulate
611 lamellae and the nuage. C. Detail of the circular arrangement of the cytoplasmic
612 membranes containing mitochondria. D. Detail of the annulate lamellae closely
613 associated to the nucleus, which still presents synaptonemal complexes
614 (arrowheads). E. Secondary spermatocyte showing tightly condensed chromatin in
615 the nucleus. The cytoplasm contains several vesicles of endoplasmic reticulum, and
616 the nuage is still present. AL, annulate lamellae; ER, endoplasmic reticulum; M,
617 mitochondria; N, nucleus; Ng, nuage.
618 Fig. 4. Maja brachydactyla. Transmission electron micrographs of spermatids. A. Early
619 spermatid showing the nucleus, located in the nuclear pole, with few clumps of
620 condensed chromatin. Note the circular arrangement of the cytoplasmic membrane
621 in the left region of the acrosome pole. B. Detail of the acrosomal pole of an early
622 spermatid showing small mitochondria and longitudinal cisternae of the
623 endoplasmic reticulum. Nuclear envelope pores (arrowhead) are oriented towards
624 the acrosomal pole. Inset shows nuclear pores (arrowheads) at higher magnification.
625 C. Seminiferous tubule showing some mid-spermatids with decondensed chromatin

and an accessory cell with oval nucleus. The cytoplasm of the accessory cells extends between spermatids, with areas of high electron-density (arrows). D. Mid-spermatids showing the nuclei with small clumps of condensed chromatin (arrowhead, also in E). In the cytoplasm, the annulate lamellae are associated to the nuclear envelope. E. Mid-spermatid showing annulate lamellae (left) and the endoplasmic reticulum (right) associated to the nucleus. The proacrosomal vesicle is formed in the acrosomal pole and contains granular homogeneous material. F. Detail of the Golgi complex of a mid-spermatid producing vesicles of light and medium electron-dense materials. AC, accessory cell; AL, annulate lamellae; AP, acrosomal pole; ER, endoplasmic reticulum; EV, vesicles of electron-dense material; GC, Golgi complex; LV, vesicles of light electron-dense material; M, mitochondria; N, nucleus; NP, nuclear pole; PV, proacrosomal vesicle.

Fig. 5. Maja brachydactyla. Transmission electron micrographs of mid-spermatids. A. Polarized spermatid containing the electron-dense granule in the apical region of the proacrosomal vesicle. B. Detail of the cytoplasm with tightly packed cisternae of the Golgi complex and adjacent mitochondria. The cytoplasm of the accessory cells, containing mitochondria (arrowhead), is intercalated between the spermatids. C. Detail of the electron-dense granule surrounded by a thin membrane (white arrows). D. Detail of the apical granule already merged into the proacrosomal vesicle. E. General view of a spermatid at the end of the mid-spermatid stage showing the discontinuous nuclear envelope (arrowheads) in the equatorial region and the degeneration of the Golgi complex. F. Detail of a degenerating Golgi complex with

adjacent mitochondria. G, granule; GC, Golgi complex; M, mitochondria; N, nucleus; PV, proacrosomal vesicle.

Fig. 6. Maja brachydactyla. Transmission electron micrographs of late spermatids. A. Several late spermatids accompanied by an accessory cell. The nucleus of the accessory cell is electron-dense, and its cytoplasm surrounds the spermatids. B. Spermatid showing the half-moon shaped nucleus, the reduced cytoplasm, and the proacrosomal vesicle. The apical region of the proacrosomal vesicle already presents the operculum, while a band of fine granular material (arrowhead) appears in the base. C. Detail of the membrane system and degenerate mitochondria, similar to the mitochondria (asterisk) that belong to the accessory cell. D. Detail of the basal region in the proacrosomal vesicle. The perforatorium is developed in association to the band of fine granular material. E. Spermatid with the nucleus surrounding the proacrosomal vesicle. The operculum extends laterally, and the granule surrounds the perforatorium following the central axis of the spermatid. An electron-dense spherical body in the cytoplasm of the accessory cell seems to be an endosomal vesicle with degradative activity. F. Spermatid showing the aggregation (white arrowheads) of the proacrosomal vesicle materials. G. Spermatid with the nucleus already showing lateral arms (arrowhead) and the uncondensed, outer layer of the proacrosomal vesicle. AC, accessory cell; EnV, endosomal vesicle of the accessory cell; G, granule; M, mitochondria; MS, membrane system; N, nucleus; P, perforatorium; PV, proacrosomal vesicle; Op, operculum.

Fig. 7. Maja brachydactyla. A. Light microscopy micrograph (H-E stain) of the seminiferous tubule. Transverse section showing the newly formed spermatozoa

671 moving from the transformation to the evacuation zone through a discontinuity in
672 the wall that separates both zones (arrow). B. Transmission electron micrograph of a
673 spermatozoon showing the typical brachyuran structure composed of a cup-shaped
674 nucleus and a globular, 3-layered acrosome centrally crossed by the perforatorium
675 and apically covered by the operculum. A1, external acrosomal layer; A2,
676 intermediate acrosomal layer; A3, inner acrosomal layer; Arm, lateral arm of the
677 nucleus; EZ, evacuation zone; N, nucleus; Op, operculum; P, perforatorium; SO,
678 structures-organelles complex; TZ, transformation zone.

TABLE 1. Characteristics of the germ cells during M. brachydactyla spermatogenesis.

	Spermatocyte	Spermatid			Spermatozoa
		Early	Mid	Late	
Cellular diameter C (µm)	12.81 ± 1.44	8.50 ± 1.82	8.08 ± 2.58	6.94 ± 0.71	4.32 ± 0.48
Nuclear diameter N (µm)	9.17 ± 1.44	6.54 ± 1.66	5.47 ± 2.28	0.99 ± 0.51	n.d.
Ratio N/C	0.72	0.77	0.68	0.14	n.d.

Data is shown as mean ± S.D. n.d., no data.

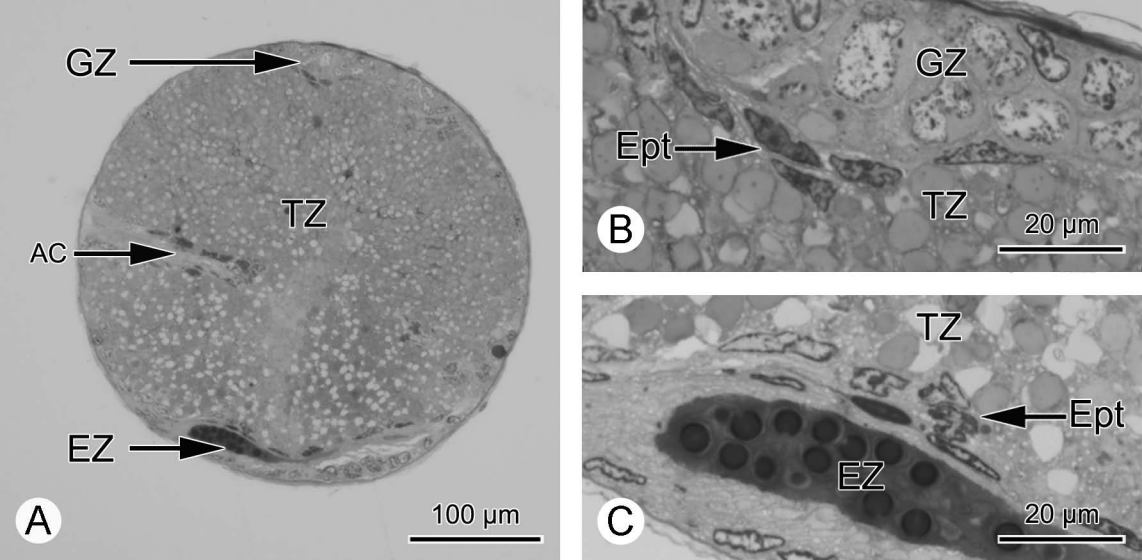
GZ
TZ
AC
EZ
A
100 µm
GZ
Ept
TZ
B
20 µm
TZ
Ept
EZ
C
20 µm

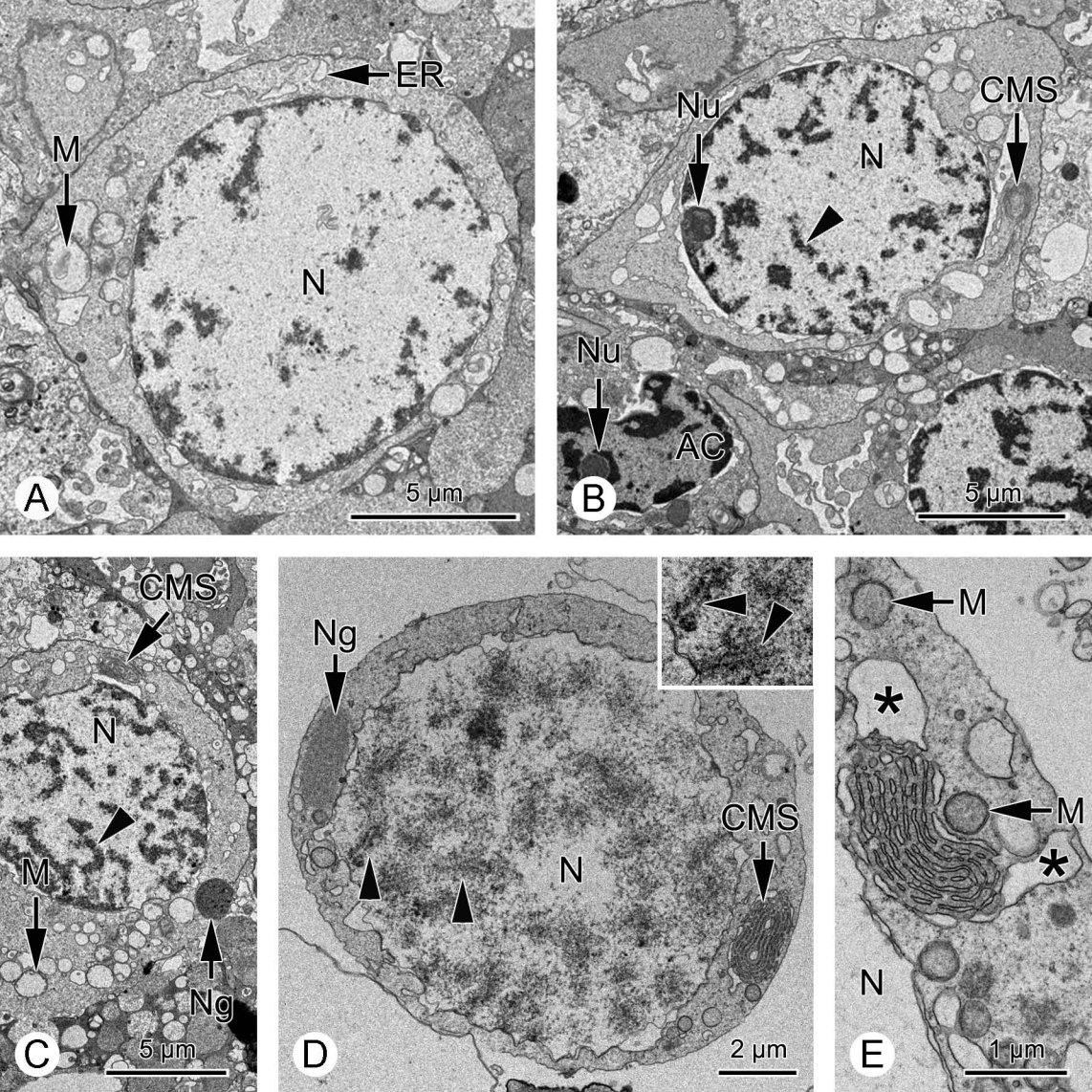
ER
M
N
A
5 µm
Nu
CMS
N
Nu
AC
B
5 µm
CMS
N
M
Ng
C
5 µm
Ng
N
CMS
D
2 µm
M
*
M
*
N
E
1 µm

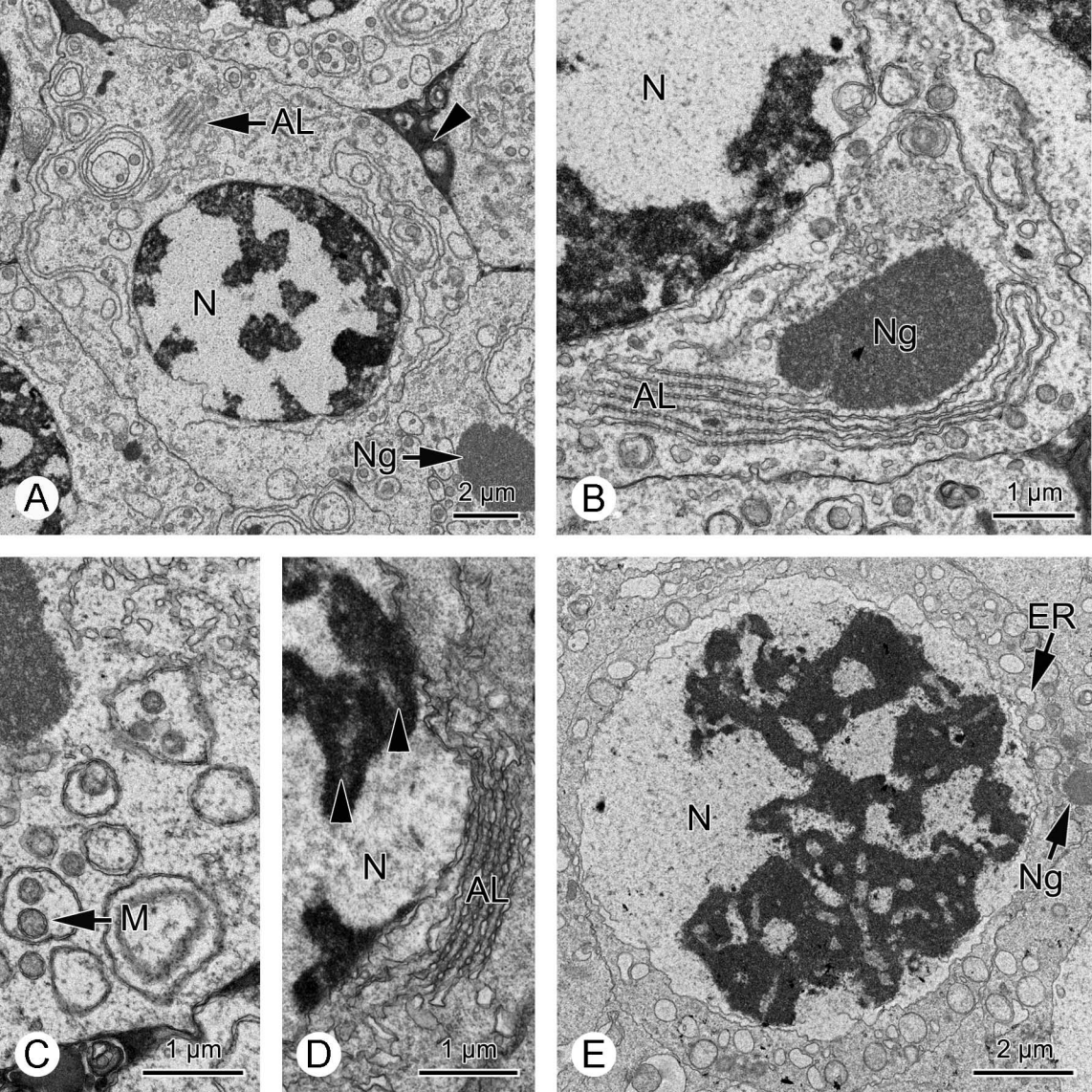
AL
N
Ng
2 µm
A
N
Ng
AL
1 µm
B
M
1 µm
C
N
AL
1 µm
D
ER
N
Ng
2 µm
E

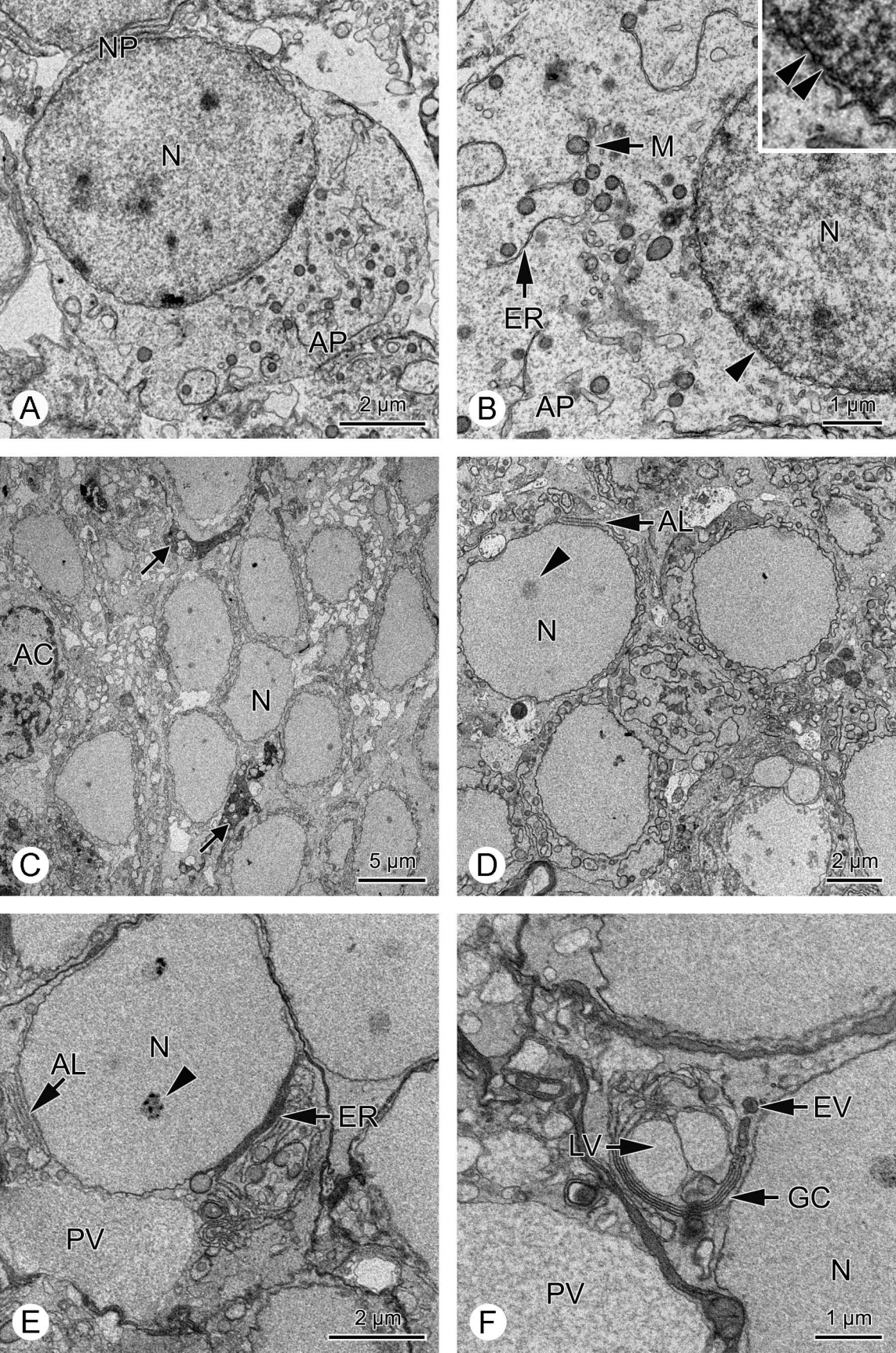
NP
N
AP
A
2 µm
M
N
ER
AP
B
1 µm
AC
N
C
5 µm
AL
N
D
2 µm
AL
N
ER
PV
E
2 µm
EV
LV
GC
N
PV
F
1 µm

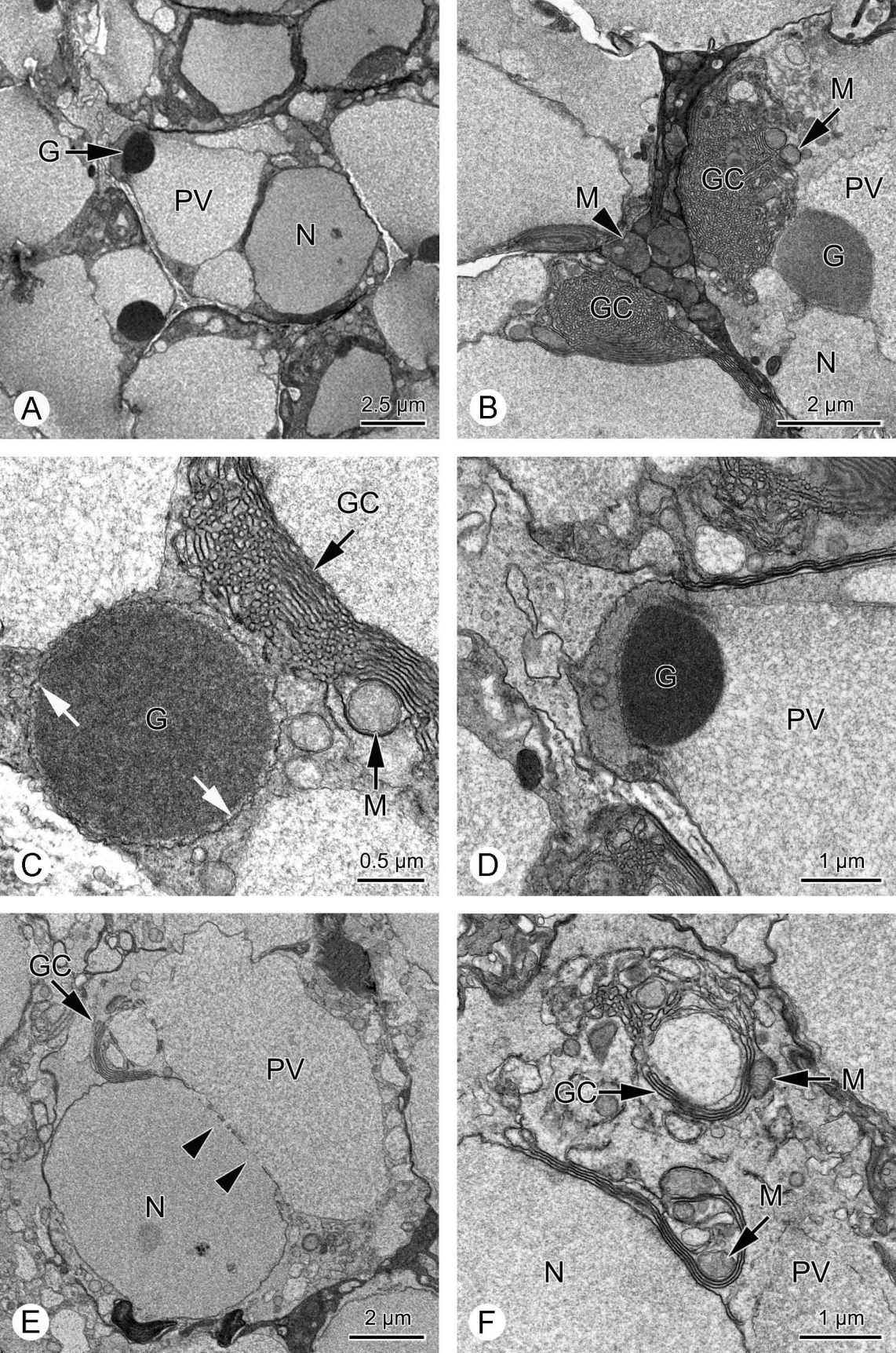
G
PV
N
2.5 µm
A
M
GC
PV
M
G
GC
N
2 µm
B
GC
G
M
0.5 µm
C
G
PV
1 µm
D
GC
PV
N
2 µm
E
GC
M
M
N
PV
1 µm
F

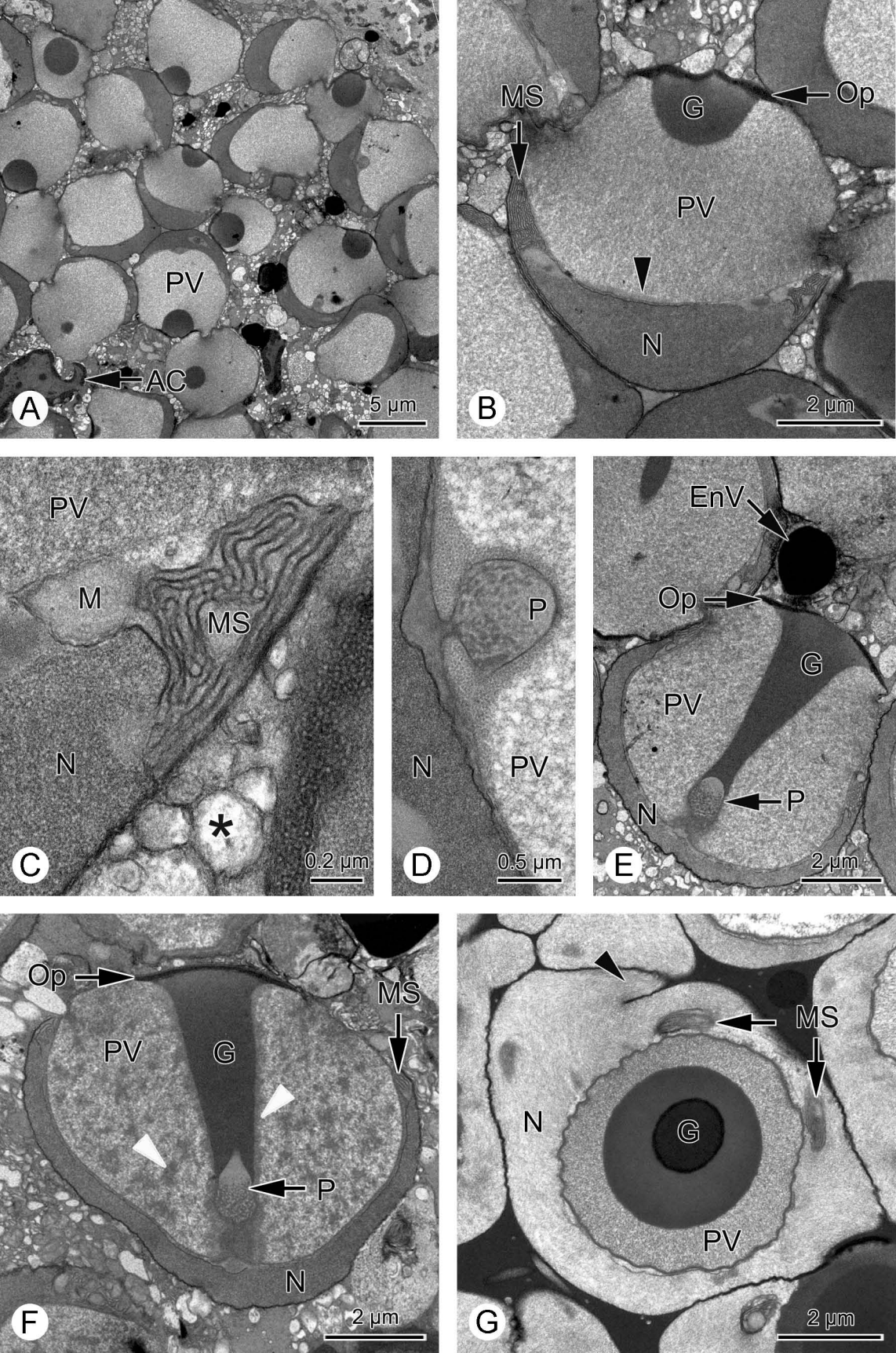
PV
AC
A
5 µm
MS
G
Op
PV
N
B
2 µm
PV
M
MS
N
*
C
0.2 µm
P
N
PV
D
0.5 µm
EnV
Op
G
PV
N
P
E
2 µm
Op
MS
PV
G
P
N
F
2 µm
MS
N
G
PV
G
2 µm

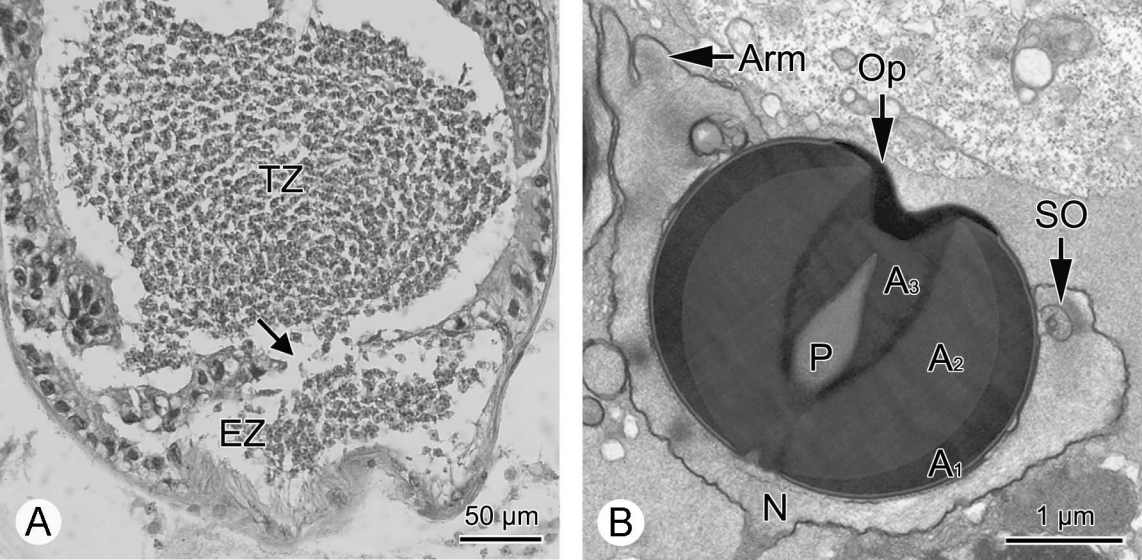
TZ
EZ
A
50 µm
Arm
Op
SO
A3
P
A2
A1
N
B
1 µm